

## Original article

# Cross-scale analysis on shale oil initiation in nanopores: Insights into threshold pressure gradient

Fenglu Cui<sup>1</sup>, Siwei Meng<sup>2</sup>, Xu Jin<sup>2</sup>, Jianhao Qian<sup>3</sup>, He Liu<sup>2</sup>, Heng'an Wu<sup>1</sup>, Fengchao Wang<sup>1</sup>

<sup>1</sup>Department of Modern Mechanics, University of Science and Technology of China, Hefei 230027, P. R. China

<sup>2</sup>PetroChina Research Institute of Petroleum Exploration & Development, Beijing 100083, P. R. China

<sup>3</sup>Department of Civil and Environmental Engineering, Rice University, Houston 77005, USA

### Keywords:

Threshold pressure gradient  
initiation  
interface effect  
size effects  
shale oil

### Cited as:

Cui, F., Meng, S., Jin, X., Qian, J., Liu, H., Wu, H., Wang, F. Cross-scale analysis on shale oil initiation in nanopores: Insights into threshold pressure gradient. *Advances in Geo-Energy Research*, 2025, 16(2): 131-142.  
<https://doi.org/10.46690/ager.2025.05.05>

### Abstract:

The low permeability of shale matrices necessitates overcoming a threshold pressure gradient to initiate hydrocarbon flow, which poses a major constraint on recovery efficiency. However, the microscopic mechanisms underlying the threshold pressure gradient, particularly the roles of interfacial interactions and pore confinement, remain unclear. A comprehensive understanding of the threshold pressure gradient is essential for enhancing recovery strategies and improving shale oil extraction efficiency. This study provides a comprehensive analysis of the interfacial and size effects on the threshold pressure gradient within kerogen, quartz, and portlandite pores using molecular dynamics simulations. A method for assessing molecular thermal motion and quantifying the threshold pressure gradient was developed using molecular dynamics simulations. The results indicate that the threshold pressure gradient decreases in the order of kerogen, quartz, and portlandite pores. The adsorption characteristics of shale oil components at the interface were clarified through density distribution and molecular behavior analysis, and the factors contributing to the threshold pressure gradient were identified. It was found that the threshold pressure gradient is significantly influenced by the strength of interfacial interactions between the polar shale oil components and the solid matrix. Additionally, an analytical model was proposed to predict the correlation between the threshold pressure gradient and the pore size, which can extend the prediction of the threshold pressure gradient to a larger scale of thousands of nanometers. These findings offer insights into shale oil recoverability in nanopores and provide theoretical guidance for its extraction.

## 1. Introduction

The understanding and theoretical modelling of nanoflow have become a hot and challenging frontier (Shahbabaie and Kim, 2021; Liu et al., 2024), not only because of the breakdown of the continuum mechanics theory (Kavokine et al., 2021), but also due to the urgent need in emerging technologies such as memory transistors (Jang et al., 2014), separation (Zhang et al., 2022), and sieving (Zhang et al., 2021). In nanoconfined environments, molecular interactions, surface/wall effects, and external forces combine to determine

whether the fluid can overcome the resistance and initiate the flow. The initiation behavior of fluids with different properties in nanopores is significantly different. For Newtonian fluids, the flow velocity increases immediately after a small pressure gradient,  $G$ , is applied across the channel, as illustrated in Fig. 1(a). The pressure gradient directly impacts the flow rate of a Newtonian fluid through a porous medium, as stated by Darcy's Law. For Bingham fluids, one of the non-Newtonian fluids, the flow will start only when the applied pressure gradient exceeds a certain value (Lipscomb and

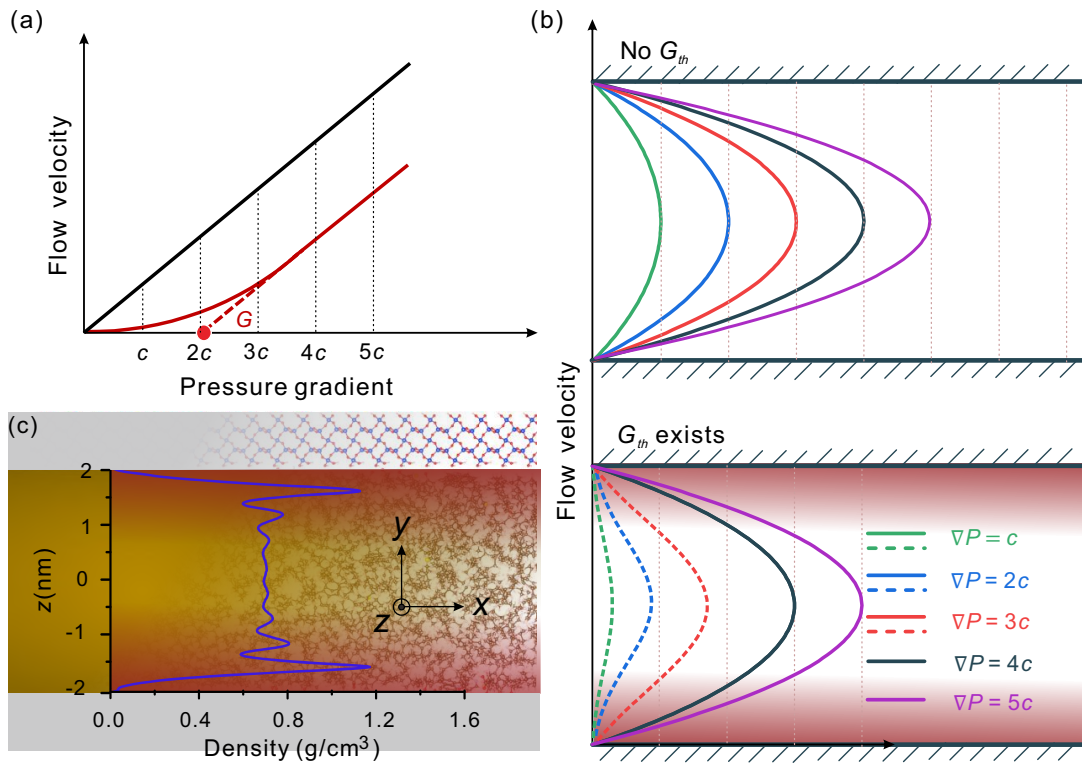


**Fig. 1.** (a) In conventional reservoirs, the flow velocity is linearly related to the pressure gradient, as described by Darcy's Law (black line). In unconventional reservoirs, the flow becomes nonlinear at lower pressure gradients (red line). The linear phase extends to zero flow velocity, and the intersection with the horizontal axis is  $G_{th}$ , (b) velocity distribution in nanopores with and without  $G_{th}$  and (c) density distribution of shale oil in a 4 nm quartz pore. A significant amount of shale oil accumulates at the interface, forming sticky layers.

Denn, 1984), which is referred to as the threshold pressure gradient,  $G_{th}$ , as illustrated in Fig. 1(a). However, when a Newtonian fluid flows through a porous medium with very low permeability (e.g., dense rock or nanopores), the interactions (e.g., adsorption, capillary forces) between the fluid and the solid wall become significantly dominant, which may impede fluid flow (Zhang, 2015; Klazly et al., 2022). Under these circumstances, a certain pressure gradient is required to overcome the resistance, which is known as the pseudo threshold pressure gradient (Rodrigues et al., 2019). The flow velocity of shale oil in nanopores under a threshold pressure gradient is much lower than it is in cases without a threshold pressure gradient, as illustrated in Fig. 1(b). In the design of oil development plans, the comprehension of  $G_{th}$  is essential because it can help determine the injection pressure and avoid wasting resources. The effectiveness of driving the oil may be compromised if the pressure gradient is lower than  $G_{th}$ . Experimental results indicate that the flow of shale oil in cores exhibits nonlinearity, proving the existence of  $G_{th}$  (Wang et al., 2011; Su, 2015). The production efficiency and economic feasibility are significantly affected, making the study of  $G_{th}$  crucial for resource evaluation, optimization of recovery strategies, and reserve estimation (Li et al., 2016).

Some studies have attempted to establish a fundamental relationship between  $G_{th}$  and rock properties from macroscopic experimental data, to provide a reference for reducing  $G_{th}$

and lowering the flow resistance (Dou et al., 2014; Wang et al., 2020; Ren et al., 2021). However, it is difficult to establish a unified and widely applicable mathematical model due to the large variation in shale oil properties across regions and the complex rock properties. Shale reservoirs exhibit low permeability and contain abundant nanopores. Nanopores are defined as pores with diameters less than 1  $\mu m$ . High-pressure mercury intrusion porosimetry experiments indicate that the dominant pore size distribution in Gulong shale oil reservoirs ranges from 10 to 50 nm, and Field Emission Scanning Electron Microscopy reveals the presence of oil within pores with a diameter of 9 nm (He et al., 2022). Therefore, it is essential to explore the nature of  $G_{th}$  from the microscopic scale. Numerous experimental results indicate an exponential relationship between  $G_{th}$  and the reservoir permeability, and  $G_{th}$  shows sensitivity to the viscosity of the shale oil (Su, 2015; Wang et al., 2020; Ren et al., 2021). From a microscopic perspective, the rock permeability corresponds to the nanopore size (Yu et al., 2020b). The viscosity of the shale oil has a significant impact on the interfacial interactions between the oil and the rock (Fan et al., 2024). It is widely believed that  $G_{th}$  is generated due to strong molecular interactions within the nanopores, resulting in the adsorption of numerous shale oil molecules onto the reservoir matrix surface, forming the sticky layers as shown in Fig. 1(c) (Wang et al., 2022). The shale oil molecules in the sticky layers need to overcome interfacial

interactions to initiate the flow. However, the underlying mechanism of interfacial interactions on  $G_{th}$  remains unclear. Studying the initiation process of shale oil in nanopores from a microscopic perspective helps to fundamentally clarify the main controlling factors of  $G_{th}$  and establish a unified evaluation standard for  $G_{th}$ .

At present, the flow behavior in nanopores is a hot topic and is being investigated by many scholars, including the applicability of Poiseuille's law at the nanoscale (Alamri et al., 2019; Alipour et al., 2019; Wang et al., 2024), the effect of interfacial slip on nanoflow (Nesterova and Gerke, 2021; Liu et al., 2022; Tomy and Dadzie, 2022), the flow state of shale oil in nanopores of different shapes and sizes (Zhu et al., 2021), and the influence of interfacial wetting behavior (Gao et al., 2021; Fan et al., 2024). Interfacial interactions have been emphasized in all these studies regarding the impact of shale oil exploitation. The adsorption behavior of shale oil at interfaces can change the occurrence state of shale oil in nanopores, affect the diffusion and flow, thereby interfering with shale oil production prediction and limiting the exploitation (Hong et al., 2022; Luo et al., 2022; Sun et al., 2023). Meanwhile, the composition of shale oil is complex. The interaction strength between the shale oil and the different reservoir matrices varies significantly (Cui et al., 2022). Therefore, the interfacial interactions pose a significant challenge for the analysis of the shale oil availability and the production prediction. Analysis of the interfacial effects on the shale oil in nanopores is crucial for understanding  $G_{th}$  of shale oil.

In this study, the initiation of the shale oil in nanopores was investigated and  $G_{th}$  was calculated. The interface effect and size effect on  $G_{th}$  were analyzed by elucidating the adsorption characteristics of shale oil components at interfaces and evaluating  $G_{th}$  in nanopores of different sizes. In addition, an analytical model was proposed to predict the relationship between  $G_{th}$  and pore size, which can extend the prediction of  $G_{th}$  to a larger scale of thousands of nanometers.

## 2. Computational methods

The initiation of shale oil in nanopores was studied using Molecular Dynamics (MD) simulations. MD simulation is a computational technique used to analyze the motion of particles in molecular or atomic systems. The simulations involve interactions between molecules or atoms, and their movements are influenced by interaction forces or potential energies determined by the force field. By following Newton's laws of motion, the particles' trajectories are captured by the simulation, which allows for the system's dynamic behavior to be captured over time. MD simulation is an important tool for studying the behavior of shale oil molecules in nanopores.

Shale oil has a complex composition, including saturated hydrocarbons, aromatics, resins, and asphaltenes (Wu et al., 2021). In this study, the molecular model of Gulong shale oil, which consists of 75% saturated hydrocarbons, 10% aromatic hydrocarbons, and 15% resins (including oxygen, nitrogen, and sulfur compounds), was used to investigate the initiation behavior of shale oil in nanopores (Cui et al., 2022). Nanopores were established by using kerogen

(Xu et al., 2021) and quartz (Qi et al., 2013), which are commonly found in shale reservoirs. The surfaces of kerogen and quartz exhibit strong oleophilicity (Cui et al., 2022). To investigate the influence of interfacial effects on the threshold pressure gradient, portlandite, which has relatively weaker oleophilicity, was chosen as a contrast, and portlandite pores were established, even though portlandite is not commonly found in shale reservoirs. Different pore sizes, including 1, 4, 10 and 20 nm, were investigated to analyze the size effect. To drive the shale oil flow, a body force was applied to the shale oil, i.e., an additional acceleration was imposed on each atom in the oil molecules. The pressure gradient can be estimated using  $\nabla P = \rho a$ , in which  $\rho$  represents the density of the shale oil, and  $a$  denotes the applied acceleration. The simulation systems were first relaxed for 1 ns in the NVT ensembles at 300 K without the pressure gradient. An 8 ns MD simulation was then performed with the pressure gradient applied. The velocity data from simulations of the last 5 ns were analyzed.

The 12-6 Lennard-Jones potential, combined with a polar term, was used to model atomic interactions, effectively considering both van der Waals and Coulombic interactions. The ClayFF force field was applied to describe the minerals (Cygan et al., 2004), while the OPLS-AA force field was used to simulate the kerogen and oil molecules (Siu et al., 2012). The mixing rule for the non-bond parameters follows the geometric method. The particle-particle-particle mesh solver is used to calculate long-range Coulombic interactions, with Fourier series evaluated to achieve a force relative error of  $1 \times 10^{-4}$  (Kelkar et al., 2007). A cutoff distance of 12 Å is applied for both van der Waals and short-range electrostatic forces. The quasi-two-dimensional flow technique adopted in this study involves the implementation of periodic boundary conditions in the  $x$  and  $z$  directions, while a fixed boundary was set in the  $y$  direction, as shown in Fig. 1(c). All the MD simulations were implemented using LAMMPS (Plimpton, 1995).

## 3. Results and discussion

### 3.1 Initiation of the nanoflow

Shale oil is stored in tight source rocks in a free or adsorbed state, with only minimal displacement or very short-range displacement in the absence of external forces. During the shale oil exploitation, molecules transition from a relatively stationary state to a directed motion under the pressure gradient. In the present study, MD simulations were employed to investigate the initiation behaviors and flow characteristics in nanopores. A pressure gradient was applied to shale oil within 4 nm pores to facilitate the investigation. It is evident that the flow velocity-pressure gradient curves exhibit significant differences in nanopores with three different matrices, suggesting different flow resistances within each pore, as shown in Fig. 2(a). The flow resistance is most pronounced in the kerogen pores, followed by the quartz pores and least in the portlandite pores. However, it remains challenging to visually distinguish the flow initiation process from the curves, particularly in identifying the transition from the nonlinear to the linear state. This limitation is due to the inherent influence of molecular thermal motion on the statistical outcomes in

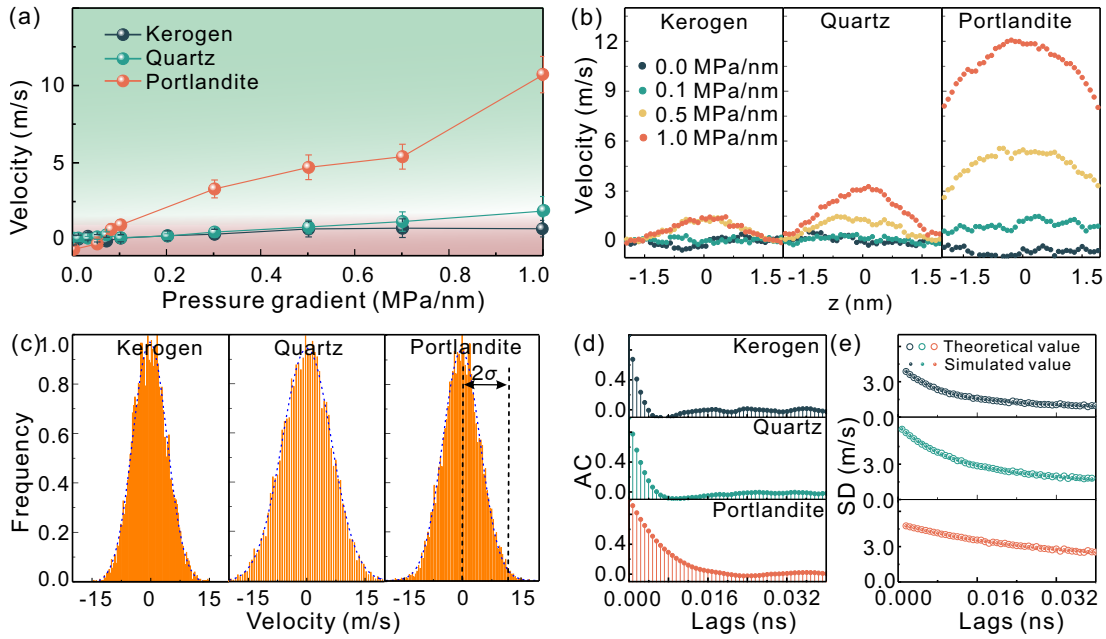


**Fig. 2.** (a) The relationship between the flow velocity of shale oil and the pressure gradient in 4 nm pores of kerogen, quartz, and portlandite, (b) the velocity distribution of shale oil in three nanopores under pressure gradients of 0.0, 0.1, 0.5 and 1.0 MPa/nm, (c) the probability distribution of molecular thermal motion velocity in three nanopores, (d) the autocorrelation function curves of velocity. Ordinate AC: Autocorrelation coefficient and (e) the standard deviation of thermal motion velocity decreases with the increasing average duration. Theoretical and simulated values (circles for theory, dots for simulations) show good consistency. Ordinate SD: Standard deviation.

MD simulations, which cannot be completely excluded. As illustrated in Fig. 2(b), the shale oil exhibits significant flow at a pressure gradient of 0.5 MPa/nm, but the flow state at a pressure gradient of 0.1 MPa/nm remains indeterminate. To evaluate  $G_{th}$  of shale oil in nanopores with different matrices, it is essential to establish a criterion that can effectively distinguish the flow behavior from the thermal motion. In the absence of an applied pressure gradient,  $10^4$  velocity data points were collected for shale oil over a total duration of 8 ns, with each data point averaged within  $\Delta t = 0.0008$  ns. Statistical results showed that the velocity distributions of the molecular thermal motions in nanopores with three different matrices all follow a Gaussian distribution, as depicted in Fig. 2(c). It was determined that, if the velocity falls within twice the standard deviation,  $2\sigma$ , there is a 95% probability that the observed motion can be attributed to molecular thermal fluctuations, which has been confirmed by statistical analysis. In contrast, velocities greater than  $2\sigma$  indicate that the shale oil has transitioned into a dynamic flow state. Therefore,  $2\sigma$  is considered as the velocity fluctuation range. However, evaluating velocity fluctuations within a duration of 5 ns requires many data points. Each data point should be obtained from the statistical analysis on an individual simulation of 5 ns, which is computationally expensive for MD simulations. Therefore, a correlation analysis of the velocity data was performed, as shown in the Fig. 2(d). The change in the standard deviation of the thermal motion velocity with increasing statistical time can be derived as:

$$\sigma_t = \frac{\sigma_0}{\sqrt{n}} \sqrt{1 + 2 \sum_{k=1}^{n-1} \left(1 - \frac{k}{n}\right) R(k)} \quad (1)$$

where  $\sigma_t$  represents the standard deviation of the thermal motion velocity at an average time  $t$ , in this study,  $t = n\Delta t$ ,  $n$  is the number of  $\Delta t$ ,  $\sigma_0$  is the standard deviation of the velocity data without the pressure gradient, and  $R(k)$  is the autocorrelation function of the velocity data without the pressure gradient. The detailed derivation is provided in the supplementary file. Eq. (1) can be validated, as shown in the Fig. 2(e), where the theoretical values derived from Eq. (1) agree well with the calculated values from MD simulations.

The velocity fluctuation range of shale oil in 4, 10 and 20 nm nanopores at a statistical time length of 5 ns was determined, as illustrated in Fig. 3(a). To evaluate the effects of interfacial interactions and pore size on  $G_{th}$ , the maximum fluctuation range (0.5 m/s) is adopted as the evaluation criterion for the shale oil initiation. When the shale oil velocity exceeds 0.5 m/s, it would transition from the thermal motion fluctuations to the directional flow. The variation of  $G_{th}$  with increasing pore size for shale oil in these three types of nanopores was analyzed based on this criterion, as shown in Fig. 3(b).  $G_{th}$  follows the order: Kerogen > quartz > portlandite. Furthermore,  $G_{th}$  exhibits an exponential decay with increasing pore diameter, consistent with the experimental observation (Liu et al., 2021).

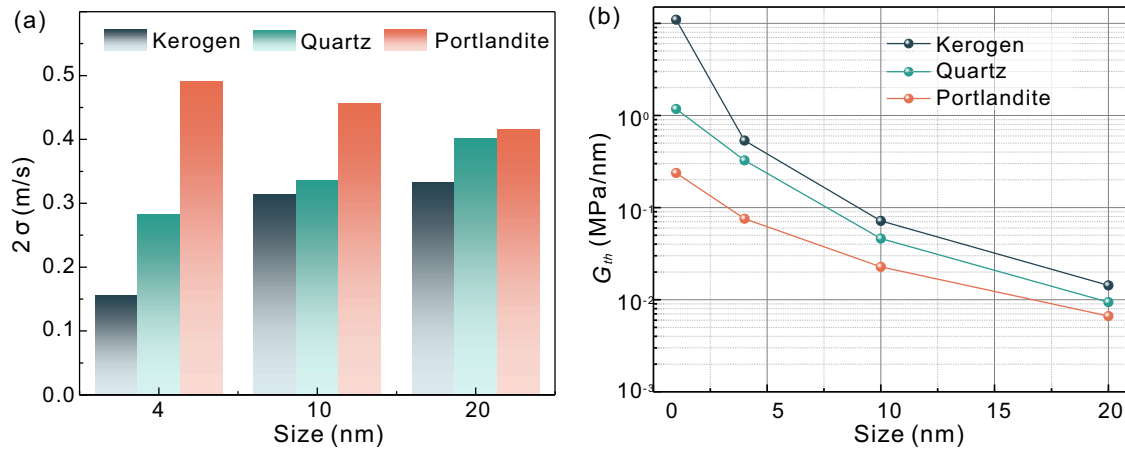


**Fig. 3.** (a) Fluctuations in the thermal motion velocities of shale oil in 4, 10 and 20 nm pores at a statistical time length of 5 ns. The vertical axis represents twice the standard deviation of the thermal motion velocity, while the horizontal axis denotes the pore size and (b) the variation of  $G_{th}$  with increasing pore size for shale oil in kerogen, quartz, and portlandite nanopores.

### 3.2 The interface effect on $G_{th}$

During shale oil exploitation, molecules transition from a relatively stationary state to a directed motion under the applied pressure gradient. Compared to the static adsorption behavior, the flow state of shale oil provides a clearer demonstration of the influence of interfacial interactions. Therefore, a large pressure gradient (1 MPa/nm) was applied to the shale oil in nanopores, which resulted in a velocity curve resembling a “parabolic” shape. However, due to the different interfacial interactions, the flow behavior of the shale oil in nanopores exhibits significant variations, mainly manifested in different flow velocities of the shale oil under the same pressure gradient. The flow state of shale oil in 4 nm pores was calculated, as shown in Fig. 4. To illustrate the flow behaviors of shale oil molecules, some shale oil molecules were marked in blue at the initial time ( $t = 0$  ns) and a pressure gradient of 1 MPa/nm was applied to the shale oil. At times  $t = 0.2$  and  $t = 0.5$  ns, the distribution of the marked shale oil molecules in three nanopores showed significant differences. In the kerogen nanopore, the shale oil molecules appear to be highly restricted, especially near the solid-liquid interface. In contrast, the shale oil flow in the quartz nanopore is much smoother. Although some shale oil molecules are restricted near the interface, those in the pore center show good flow characteristics. In contrast to the behaviors observed in the kerogen and quartz nanopores, shale oil in the portlandite pore shows high mobility, with shale oil molecules not forming stable adsorption at the interface. Overall, the flowability of shale oil in these three nanopores follows the order: Portlandite > quartz > kerogen. In addition, the roughness of the matrix surface also has a considerable impact on the flow (Papanikolaou et al., 2016). Due to the significantly higher roughness of the kerogen surface compared to the mineral surface, this further inhibits the shale oil flow in kerogen nanopores (Yu et al., 2020a).

A more intuitive representation in the flow velocity distribution of shale oil in the three nanopores at a pressure

gradient of 1 MPa/nm is provided in Fig. 5. In kerogen and quartz nanopores, shale oil near the interface is constrained and shows no significant flow, even exhibiting a “negative slip” phenomenon. In the portlandite nanopore, shale oil molecules show high mobility.

The interfacial interaction is the main factor restricting the shale oil flow (Cai et al., 2024). The closer the shale oil molecules are to the matrix surface, the stronger the interfacial interactions they experience, leading to a stable inhibition of shale oil mobility. Therefore, there is a question here: Can shale oil in nanopores be fully extracted, or in other words, how much shale oil can be easily mobilized in nanopores? As shown in Fig. 4, the shale oil in the center of nanopores is more mobilizable, while the mobilizability of shale oil near the interface is constrained by interfacial interactions. The density distribution curve of shale oil indicates a high accumulation of shale oil at the interface, which shows a pronounced layering phenomenon, as shown in Fig. 6(a). According to the density distribution, shale oil within nanopores was categorized into several research objects to investigate the interfacial interactions. The density peak closest to the interface is defined as the first layer, and those closest and next closest are referred to as the second layer, and so on. In the case of a 4 nm pore, the shale oil is roughly divided into four layers, as illustrated in Fig. 6(a). To provide a clear description of the effect of interfacial interactions on  $G_{th}$ , the layered approach was used to study the flow state of shale oil in kerogen, quartz, and portlandite nanopores. Shale oil was divided into four layers in 4 nm pores. As expected, stronger interfacial interactions result in higher  $G_{th}$ , as illustrated in Fig. 6(b). In kerogen nanopores,  $G_{th}$  for the first layer of shale oil reaches 3.7 MPa/nm, which is significantly higher than  $G_{th}$  for shale oil in quartz and portlandite nanopores. As the distance from the interface increases, the strength of interfacial interactions gradually weakens, and  $G_{th}$  decreases rapidly. This decay is most pronounced in the kerogen nanopore. In contrast, the difference in  $G_{th}$  between the first layer and the fourth layer

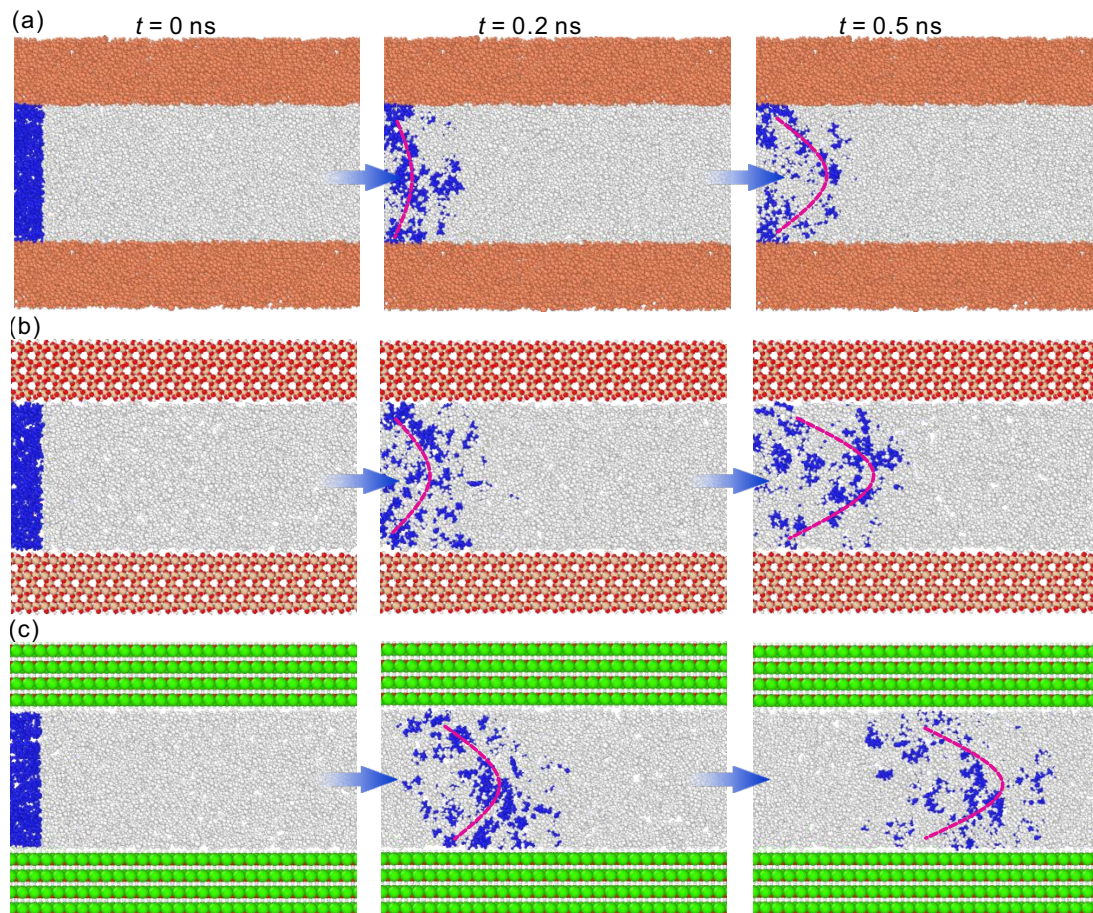


**Fig. 4.** The flow state of shale oil in 4 nm nanopores at a pressure gradient of 1 MPa/nm. The blue color represents shale oil molecules marked at the initial moment ( $t = 0$  ns), and these molecules are shown at  $t = 0.2$  and  $0.5$  ns. (a) Kerogen nanopore, (b) quartz nanopore and (c) portlandite nanopore.

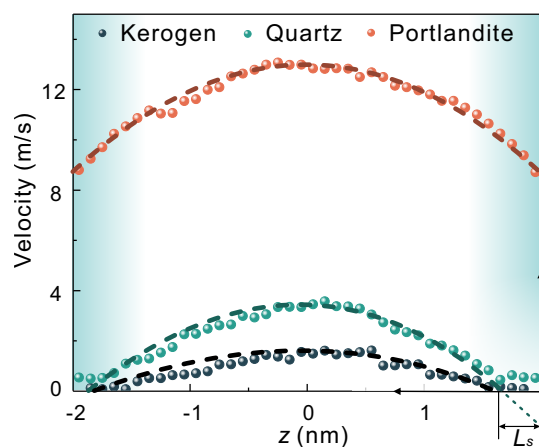


**Fig. 5.** The flow velocity distribution of shale oil in 4 nm nanopores. The dashed parabola represents the fitted curve of MD results, while  $L_s$  is the extension of the green dashed line to the pore boundary, indicating a negative slip length.

of shale oil molecules is relatively small in the portlandite nanopore. Thus, it is challenging to fully recover shale oil from nanopores in shale oil exploitation due to the influence of interfacial interactions. Different reservoir matrix pores have

different recoverable volumes of shale oil, influenced by interfacial interactions. In shale reservoirs, numerous mesopores and micropores are interwoven, with shale oil molecules filling the spaces. Under the driving force of the production pressure differential, shale oil molecules with minimal interfacial interactions are mobilized first. When the driving force provided by the production pressure differential is insufficient to free the shale oil molecules from the constraints of the reservoir matrix, effective exploitation cannot occur. For example, during the shale oil exploitation process, if a driving pressure gradient of 1 MPa/nm is applied, shale oil in 4 nm portlandite pores can be fully extracted, shale oil in 4 nm quartz pores can be extracted approximately 90%, while the effective recoverable volume of shale oil in 4 nm kerogen pores is only 50%. Therefore, the analysis of  $G_{th}$  in nanopores for shale oil contributes to theoretical assessment of the recoverable volume of reservoirs.

Through this layer analysis, it was found that the thickness of the sticky layer formed by shale oil varies across three matrix surfaces, which significantly affects the effective pore size. The thicknesses of the first sticky layer in kerogen, quartz, and portlandite pores are 0.495, 0.380 and 0.365 nm, respectively, as illustrated in the Fig. 6(b). The distribution of different component densities in shale oil inside the nanopore

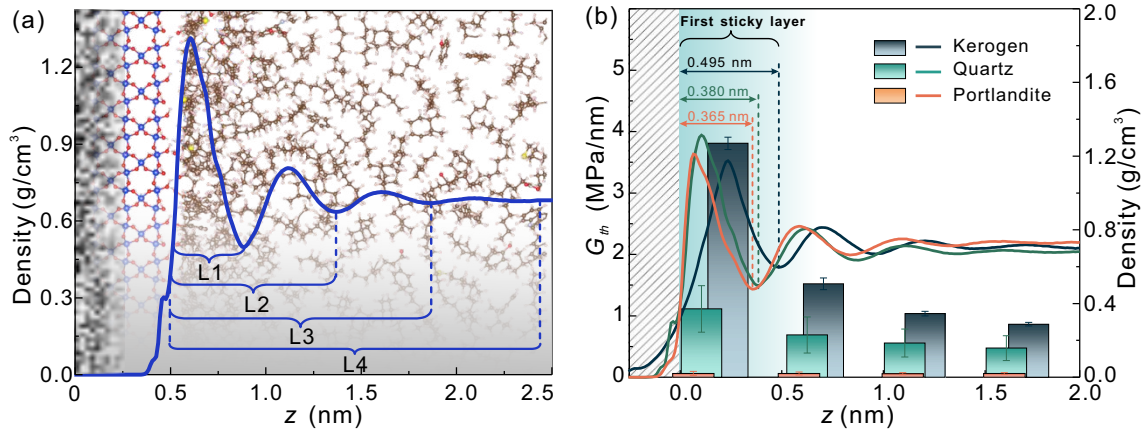


**Fig. 6.** (a) The stratification of shale oil in a 4 nm nanopore according to the density distribution and (b) the bar chart represents  $G_{th}$  of shale oil in three nanopores, while the curves depict the density distribution of shale oil.

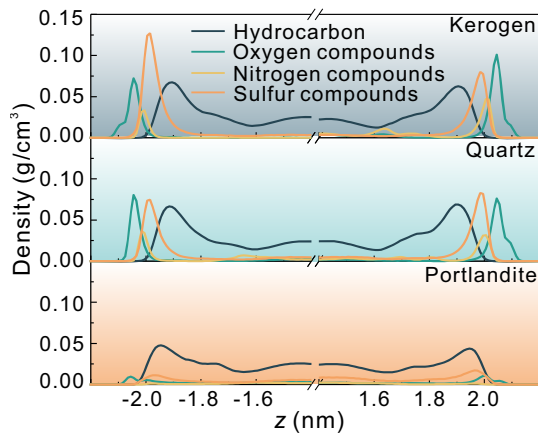


**Fig. 7.** The density distribution of shale oil components in 4 nm nanopores.

res was analyzed, as shown in Fig. 7. Obviously, in kerogen and quartz pores, a significant concentration of polar molecules, especially oxygen compounds, is observed near the interface. The distribution is thought to indicate strong interactions between these polar molecules and the solid matrix. Conversely, in portlandite pores, there is no notable difference in the interfacial adsorption of polar compounds and hydrocarbon compounds. Therefore, the strong interactions between polar compounds and the solid matrix are identified as a significant factor leading to  $G_{th}$ .

To illustrate the interactions between the shale oil molecules and the solid matrix, the adsorption and desorption behaviors of the shale oil molecules on the solid matrix surface were analyzed, and the states of the shale oil molecules at different times were recorded, as shown in Fig. 8. In kerogen nanopores, shale oil components tend to form stable adsorption at the interface. Under the driving force of pressure gradients, shale oil molecules adsorbed at the interface gradually undergo slight changes in the adsorption angles. The adsorption angle refers to the angle between the orientation of the molecular skeleton and the wall surface. As depicted in Fig. 8(a), at  $t = 0$  ns, the polar components adsorb vertically at the

interface, and at  $t = 0.5$  ns, the adsorption angle changes to  $110^\circ$ . The small change in the adsorption angle maintains a relatively high level of resistance to the flow of shale oil. In contrast, at the quartz interface, the polar components undergo more significant angle changes under the driving force of pressure gradients, as shown in Fig. 8(b), which undoubtedly reduces the resistance to flow. In addition, due to the higher roughness of the kerogen surface compared to the surface of inorganic minerals, shale oil molecules experience a greater adsorption area at the interface, leading to greater difficulty in the desorption of shale oil molecules. In quartz pores, the interface cannot stably capture the adsorbed hydrocarbon compounds. Under the driving force, hydrocarbon compounds can more easily achieve desorption, as shown in Fig. 8(b). In contrast, both polar and non-polar shale oil components do not show stable adsorption behavior at the portlandite interface, as shown in Fig. 8(c). This explains why shale oil in portlandite pores exhibits very high flow velocity under the same pressure gradient, as shown in Fig. 5.

During the flow of shale oil molecules in nanopores, adsorption and desorption behaviors occur continuously. The state changes of the shale oil molecules during the flow process were recorded to illustrate the adsorption and desorption behaviors, as shown in Fig. 9. The vertical axis represents the position coordinates of shale oil molecules perpendicular to the flow direction over time. In kerogen and quartz pores, shale oil molecules exhibit three types of behaviors, as depicted in Fig. 9(a). Type 1 curve indicates that the shale oil molecules do not consistently adsorb at the interface, which demonstrates good fluidity. The type 2 curve represents that the shale oil molecules intermittently adsorb at the interface during the flow process and detach from the interface due to the driving pressure gradient and molecular thermal motion. As for the type 3 curve, the shale oil molecules, once adsorbed at the interface, reached a stable state without further desorption. In kerogen pores, the molecular states are predominantly characterized by types 1 and 3, whereas in quartz pores, states are mainly represented by types 1 and 2. In portlandite pores, shale oil molecules flow in two types, as shown in Fig. 9(b).

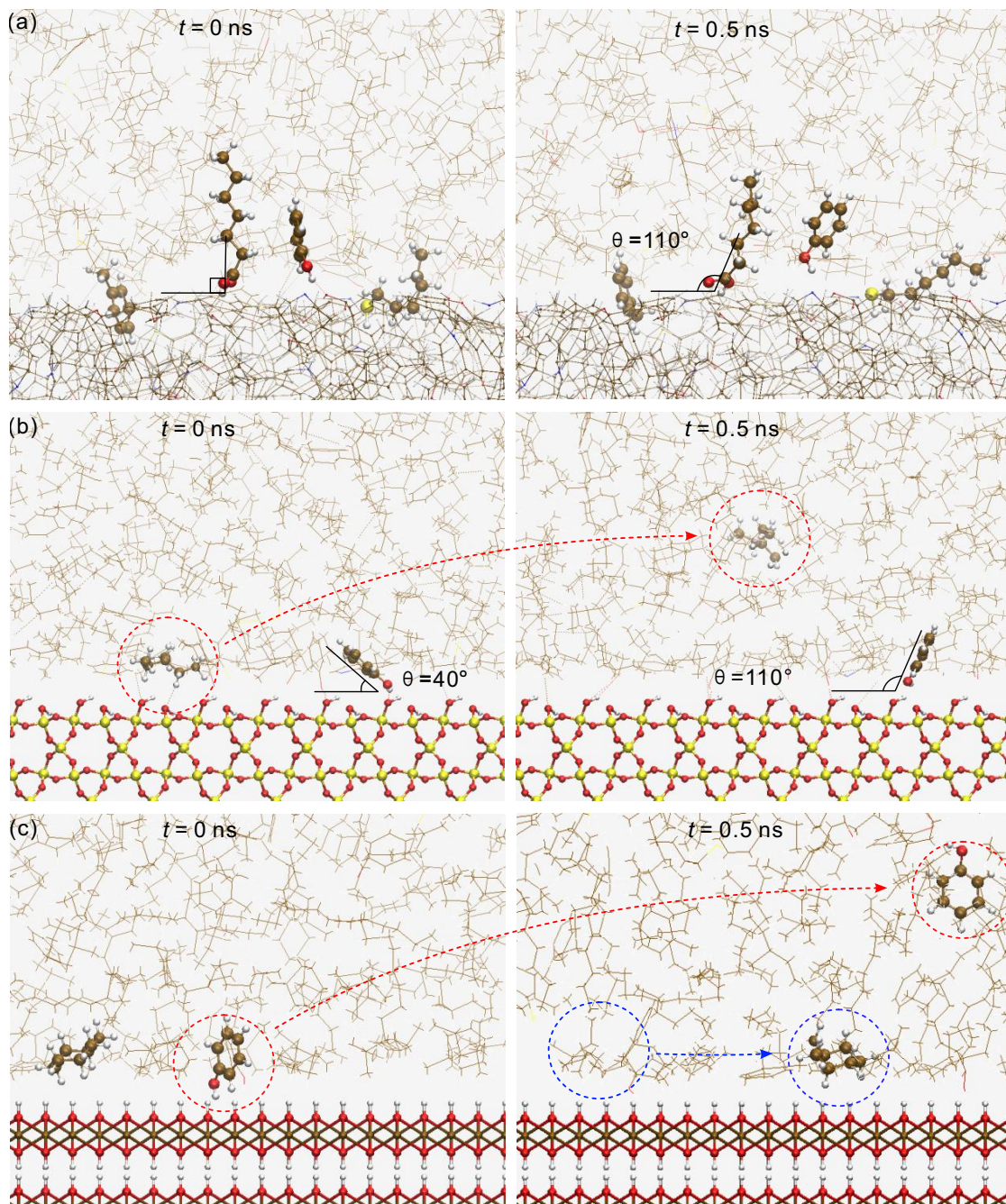


**Fig. 8.** The adsorption states of shale oil molecules on the surfaces of three matrixes at  $t = 0$  and  $t = 0.5$  ns. (a) Kerogen surface, (b) quartz surface and (c) portlandite surface.

The type 1 curve in Fig. 9(b) is the same as the type 1 curve in Fig. 9(a). The type 4 curve involves shale oil molecules that exhibit behavior similar to the specular reflection at the interface, which is conducive to the flow (Qian et al., 2023). The weaker interfacial interactions cannot capture shale oil molecules in portlandite pores.

In summary,  $G_{th}$  of shale oil is affected by the strength of interfacial interactions between the polar shale oil components and the solid matrix, which also influences the recoverable volume of shale oil in nanopores to some extent.

### 3.3 The size effect on $G_{th}$

Shale reservoirs have a complex pore structure. Taking the Gulong shale as an example, the predominant microscale pores are in the range of 10-50 nm (He et al., 2022). The effect of interfacial interactions with an increasing pore size on the shale oil availability is unknown. Here,  $G_{th}$  of three different nanopores with various sizes were summarized, as shown in Fig. 10.  $G_{th}$  was obtained by analyzing the velocity in the first sticky layer as defined in Fig. 6(a). For all the pore sizes,  $G_{th}$  follows the order: Kerogen > quartz > portlandite. The results indicate that  $G_{th}$  decreases rapidly as the pore size increases.

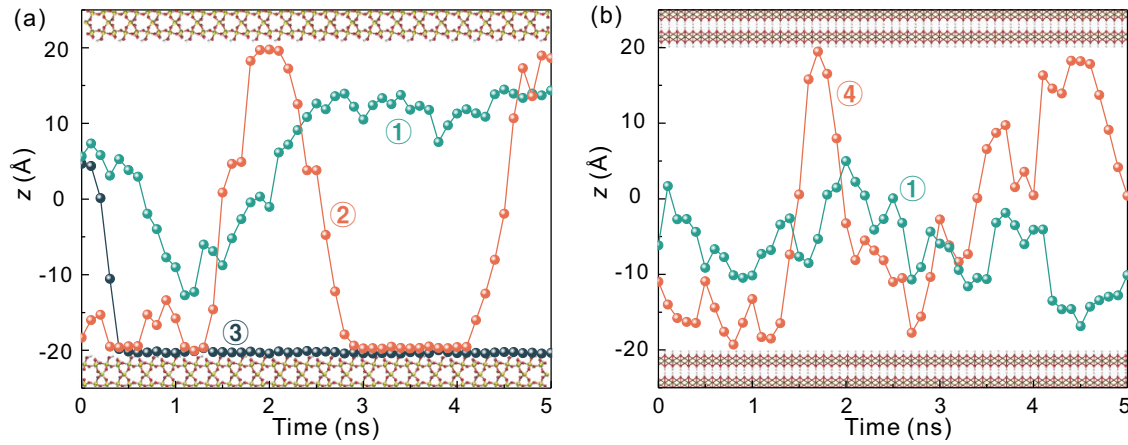


**Fig. 9.** The flow trajectories of shale oil molecules in nanopores. (a) Flow trajectories of shale oil in kerogen pores and quartz pores, which are similar and (b) the flow trajectories of shale oil molecules in portlandite pore.

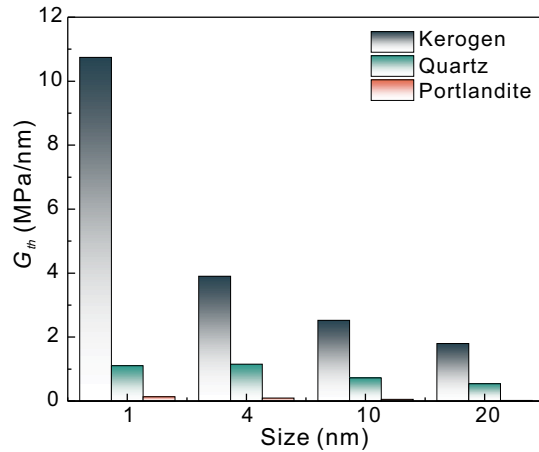


**Fig. 10.** (a) Variations in  $G_{th}$  in the first sticky layer of three different nanopores with various size.

For kerogen nanopores,  $G_{th}$  of 1 nm pore is 6.0 times larger than  $G_{th}$  of 20 nm pore. In addition, the variations in  $G_{th}$  at different positions in nanopores with sizes of 10 and 20 nm were also analyzed. The results were summarized in Fig. 11. Due to the relatively uniform density in the central part of 10 and 20 nm pores, it is difficult to accurately define the layers there. Therefore, shale oil in the 10 and 20 nm pores was divided using a thickness of 1 nm. In both 10 and 20 nm pores,  $G_{th}$  exhibits a rapid decay as the distance of shale oil molecules from the interface increases. This is because the interactions between the solid matrix and the shale oil molecules in the intermediate layer of the pore become negligible.  $G_{th}$  of the intermediate layer is mainly determined by the interactions among shale oil molecules (liquid/liquid interactions). Furthermore,  $G_{th}$  decays faster with position in kerogen nanopores. For 10 nm pores with kerogen walls,  $G_{th}$  in the first layer is 14.7 times larger than  $G_{th}$  in the central part. This ratio decreases to only 1.9 for portlandite pores of 10 nm, as shown in Fig. 11(a). For 20 nm pores with kerogen walls,  $G_{th}$  in the first layer is 33.2 times larger than  $G_{th}$  in the central part. This ratio decreases to 3.1 for portlandite pores of

20 nm, as shown in Fig. 11(b). The differences in  $G_{th}$  caused by interfacial interactions decrease as the strength of interfacial interactions weakens. It is observed that the decay in  $G_{th}$  at different positions from the solid/liquid interface to the central part is more significant for 20 nm nanopores.

### 3.4 A cross-scale theory model on $G_{th}$

MD simulations are limited by the spatial scale, making it difficult to model the fluid flow in larger pores. Here, an alternative approach is taken to understand the shale oil initiation process from a different perspective. At the macroscopic level, when a fluid flows in a pipeline, the relative motion results in the friction between the liquid and the neighboring liquid as well as the solid wall. At the molecular level, this corresponds to the shear action occurring between molecules. Thus, the liquid flow is essentially a process in which liquid molecules are displaced by the shear stress. Shale oil molecules undergo irregular thermal motion in the reservoir, and experience shear stress under the driving pressure gradient. If the shear stress acting on the shale oil molecules cannot distinguish the directional flow velocity from the thermal motion fluctuations, the shale oil flow will not be initiated. Therefore, there is a shear stress that allows the shale oil flow to precisely overcome the influence of molecular thermal motion, referred to as the critical shear stress  $\tau_c$ . The flow velocity of the molecules at the solid/liquid interface under the critical shear stress is the critical velocity  $V_c$ . The present study builds upon earlier research that proposed a relationship between the shear stress and the interfacial flow velocity based on the Eyring's molecular kinetic theory (Wang and Zhao, 2011):

$$\tau = Vk \quad (2)$$

where  $k$  is analogous to the friction coefficient presented in Brillouin's expression. In this study, the flow of shale oil in three different matrix pores corresponds to different values of  $k$ , which can be obtained by fitting the simulation results. When a pressure gradient  $G$  is applied to the shale oil molecules in a nanopore with a pore size of  $H$ , the shear stress

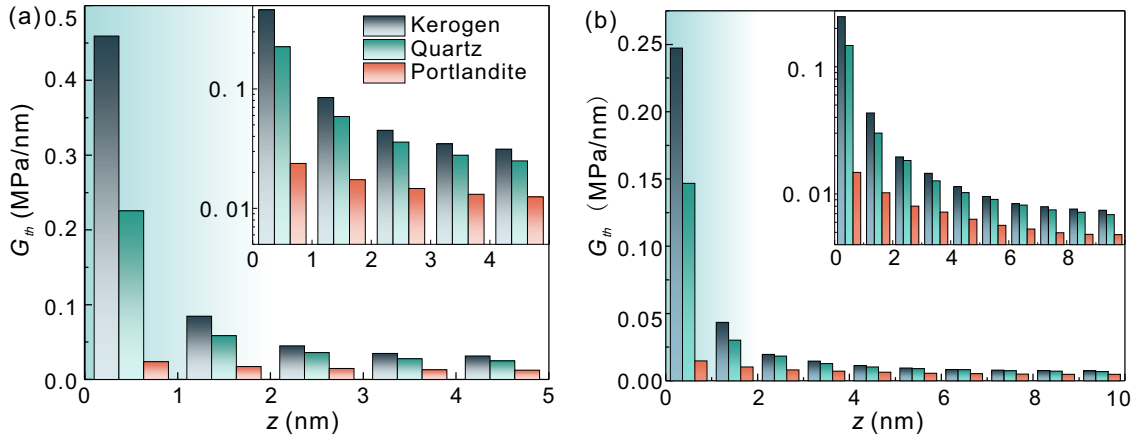


**Fig. 11.** (a) Variations in  $G_{th}$  at different positions in nanopores of 10 nm and (b) variations in  $G_{th}$  at different positions in nanopores of 20 nm. The insets in the upper right corner show  $G_{th}$  on a logarithmic scale.

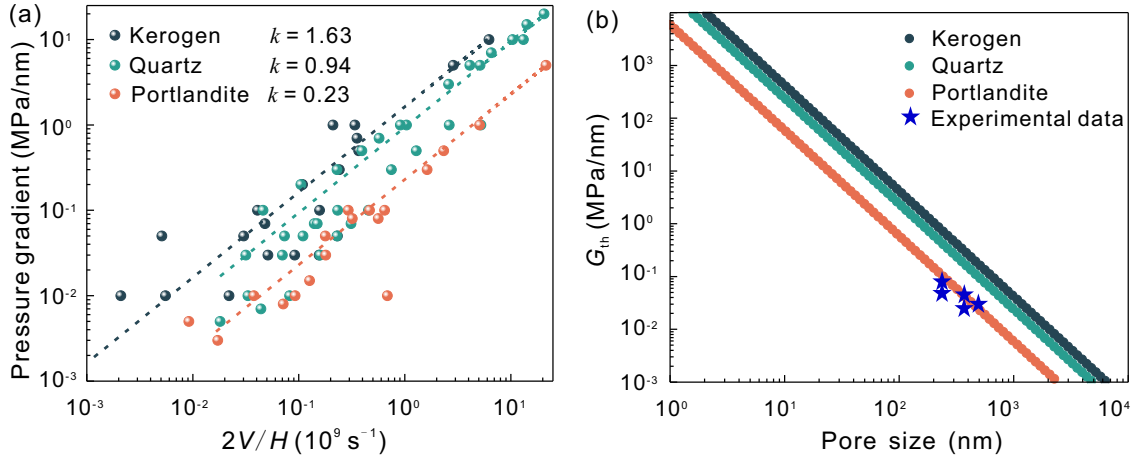


**Fig. 12.** (a) Determination of the coefficient  $k$  in MD simulations. According to Eq. (3), the applied pressure gradient  $G$  is proportional to  $2V/H$  and the slope is  $k$  and (b) the predicted  $G_{th}$  as a function of the pore size. The coefficient  $k$  was obtained by fitting MD results. The blue pentagrams represent the experimentally measured values of  $G_{th}$  (Wang et al., 2011; Su, 2015).

experienced by shale oil molecules is given by:  $\tau = GH/2$ . Thus, the relation among the applied pressure gradient, the interfacial flow velocity, and the pore size can be obtained:

$$G = \frac{2kV}{H} \quad (3)$$

The physical significance of  $k$  can be interpreted as the coefficient characterizing the difficulty of the shale oil initiation. A larger  $k$  indicates a stronger solid/liquid interaction and a more difficult initiation. In the pores of kerogen, quartz, and portlandite, the values of  $k$  are 1.63, 0.94, and 0.23, respectively, as shown in Fig. 12(a).

Eq. (3) is employed to analyze  $G_{th}$  and extend its prediction to a larger scale. To this end, the model is calibrated using experimental results. The experimental data for  $G_{th}$  of shale oil in a core with a permeability of 4.454 mD is 0.07 MPa/m (Wang et al., 2011). In accordance with the classical continuum theory for incompressible fluids (Navier-Stokes equations), the flow of shale oil in a core with a permeability of 4.454 mD can be likened to the flow in a two-dimensional slit with a size of

$H = 231.2$  nm (Yu et al., 2020b). Applying Poiseuille's law, the average flow velocity of shale oil in the 231.2 nm slit is determined to be 55.7 nm/s under a pressure gradient of 0.07 MPa/m (Sutera and Skalak, 1993). Given that 0.07 MPa/m is considered as the  $G_{th}$  for shale oil in a core with a permeability of 4.454 mD, the flow velocity of 55.7 nm/s can be regarded as the critical velocity,  $V_c$ . Furthermore, the corresponding critical flux (per unit width),  $F_c \approx HV_c$ , is 12,860.7 nm<sup>2</sup>/s.  $F_c$  was crudely considered as a standard for experimentally assessing whether the shale oil flow is initiated. At the moment of the shale oil initiation,  $V = V_c$ ,  $G = G_{th}$ . Thus:

$$G_{th} = \frac{2kF_c}{H^2} \quad (4)$$

Using Eq. (4), the relationship between  $G_{th}$  and the pore size  $H$  were plotted for three different matrices, as shown in Fig. 12(b). Theoretical results were compared with some experimental data, and achieved a good agreement (Su, 2015; Wang et al., 2011), which indicates that the predictive model for  $G_{th}$  is reliable. In this model, the averaged flow velocity

of all shale oil in the nanopore was utilized to obtain  $G_{th}$  for the overall shale oil. Similarly, by using the flow velocity of shale oil in each layer,  $G_{th}$  can be obtained for each layer. By comparing the  $G_{th}$  of each layer of shale oil with the production pressure difference, the recoverable reserves of shale oil in the pore can be determined. In addition, another significant advantage of this model is that the coefficient  $k$  can be determined in MD simulations on a relatively small system, allowing for the prediction of  $G_{th}$  of shale oil flow in large pores, even those larger than  $10^3$  nm.

#### 4. Conclusions

Fluid behavior in confined nanopores is strongly influenced by interfacial interactions, which can be exacerbated by the confinement effect. To investigate the initiation of the shale oil flow within nanopores, a MD based method was developed for evaluating thermal motion fluctuations, which was further applied to quantify the  $G_{th}$  of shale oil in nanopores.  $G_{th}$  of shale oil in kerogen, quartz, and portlandite nanopores was calculated to analyze the interface effect on the  $G_{th}$ . The results show that  $G_{th}$  follows the order: Kerogen > quartz > portlandite. The stable and intermittent adsorption behaviors of polar shale oil molecules at interfaces are key factors contributing to the higher  $G_{th}$ . The size effect on  $G_{th}$  was also investigated. As the pore size increases (1, 4, 10 and 20 nm),  $G_{th}$  of shale oil shows a significant decrease. It was also found that  $G_{th}$  exhibits a rapid decay as the distance of shale oil molecules from the interface increases. This is because the interactions between the solid matrix and the shale oil molecules in the intermediate layer of the pore become negligible. An analytical model was proposed to predict the relationship between  $G_{th}$  and the pore size, which can extend the prediction of  $G_{th}$  to a larger scale of thousands of nanometers. The model shows that  $G_{th}$  is inversely proportional to the square of the pore size. In practical application, the coefficient  $k$  can be determined in MD simulations on a relatively small system and then used to predict  $G_{th}$  of the shale oil flow in large pores. Overall, the initiation of the shale oil flow within nanopores is of great importance for the reservoir reserve assessment and economic feasibility. This study addresses the gap in experimental understanding of microscopic flow mechanisms, providing new insights into interfacial interactions that influence flow initiation. The findings offer a theoretical reference for optimizing injection pressure parameters in shale oil recovery.

#### Acknowledgements

This work was financially supported by the National Natural Science Foundation of China (Nos. U22B2075, 12241203, 123B2029 and 12102421). The numerical calculations were performed on the supercomputing system in Hefei Advanced Computing Center and the Supercomputing Center of University of Science and Technology of China.

#### Additional information: Author's email

wangfc@ustc.edu.cn (F. Wang).

#### Conflict of interest

The authors declare no competing interest.

**Open Access** This article is distributed under the terms and conditions of the Creative Commons Attribution (CC BY-NC-ND) license, which permits unrestricted use, distribution, and reproduction in any medium, provided the original work is properly cited.

#### References

- Alamri, S. Z., Ellahi, R., Shehzad, N., et al. Convective radiative plane Poiseuille flow of nanofluid through porous medium with slip: An application of Stefan blowing. *Journal of Molecular Liquids*, 2019, 273: 292-304.
- Alipour, P., Toghraie, D., Karimipour, A. Modeling different structures in perturbed Poiseuille flow in a nanochannel by using of molecular dynamics simulation: Study the equilibrium. *Physica A: Statistical Mechanics and its Applications*, 2019, 515: 13-30.
- Cai, J., Jiao, X., Wang, H., et al. Multiphase fluid-rock interactions and flow behaviors in shale nanopores: A comprehensive review. *Earth-Science Reviews*, 2024, 257: 104884.
- Cui, F., Jin, X., Liu, H., et al. Molecular modeling on Gulong shale oil and wettability of reservoir matrix. *Capillarity*, 2022, 5(4): 65-74.
- Cygan, R. T., Liang, J. J., Kalinichev, A. G. Molecular models of hydroxide, oxyhydroxide, and clay phases and the development of a general force field. *Journal of Physical Chemistry B*, 2004, 108(4): 1255-1266.
- Dou, H., Ma, S., Zou, C., et al. Threshold pressure gradient of fluid flow through multi-porous media in low and extra-low permeability reservoirs. *Science China Earth Sciences*, 2014, 57: 2808-2818.
- Fan, J., Fan, J., Hong, X., et al. Exploring wettability variations on minerals surfaces: Insights from spreading coefficient and interaction energy analysis. *Geoenergy Science and Engineering*, 2024, 234: 212672.
- Gao, Y., Wu, K., Chen, Z., et al. Effect of wetting hysteresis on fluid flow in shale oil reservoirs. *Energy & Fuels*, 2021, 35(15): 12075-12082.
- He, W., Meng, Q., Feng Z. et al. In-situ accumulation theory and exploration & development practice of Gulong shale oil in Songliao Basin. *Acta Petrolei Sinica*, 2022, 43(1): 1-14. (in Chinese)
- Hong, X., Xu, H., Yu, H., et al. Molecular understanding on migration and recovery of shale gas/oil mixture through a pore throat. *Energy & Fuels*, 2022, 37(1): 310-318.
- Jang, S., Hwang, E., Cho, J. H. Graphene nano-floating gate transistor memory on plastic. *Nanoscale*, 2014, 6(24): 15286-15292.
- Kavokine, N., Netz, R. R., Bocquet, L. Fluids at the nanoscale: From continuum to subcontinuum transport. *Annual Review of Fluid Mechanics*, 2021, 53(1): 377-410.
- Kelkar, M. S., Rafferty, J. L., Maginn, E. J., et al. Prediction of viscosities and vapor-liquid equilibria for five polyhydric alcohols by molecular simulation. *Fluid Phase Equilibria*, 2007, 260(2): 218-231.
- Klazly, M., Mahabaleswar, U. S., Bognár, G. Comparison

- of single-phase Newtonian and non-Newtonian nanofluid and two-phase models for convective heat transfer of nanofluid flow in backward-facing step. *Journal of Molecular Liquids*, 2022, 361: 119607.
- Li, D., Zha, W., Liu, S., et al. Pressure transient analysis of low permeability reservoir with pseudo threshold pressure gradient. *Journal of Petroleum Science and Engineering*, 2016, 147: 308-316.
- Lipscomb, G., Denn, M. Flow of Bingham fluids in complex geometries. *Journal of Non-Newtonian fluid mechanics*, 1984, 14: 337-346.
- Liu, J., Yang, Y., Sun, S., et al. Flow behaviors of shale oil in kerogen slit by molecular dynamics simulation. *Chemical Engineering Journal*, 2022, 434: 134682.
- Liu, P., Zhao, F., Zhang, J., et al. Micro/nano flow chemistry by beyond limits manufacturing. *Chinese Chemical Letters*, 2024, 35(5): 109020.
- Liu, Q., Wu, K., Li, X., et al. Effect of displacement pressure on oil-water relative permeability for extra-low-permeability reservoirs. *ACS Omega*, 2021, 6(4): 2749-2758.
- Luo, Y., Xiao, H., Liu, X., et al. Occurrence characteristics and influential factors of movable oil in nano-pores by molecular dynamics simulation. *Colloids and Surfaces A: Physicochemical and Engineering Aspects*, 2022, 655: 130320.
- Nesterova, I. S., Gerke, K. M. Simulations of nanoscale gas flow with Knudsen diffusion and slip flow. *Mathematical Models and Computer Simulations*, 2021, 13: 971-978.
- Papanikolaou, M., Frank, M., Drikakis, D. Nanoflow over a fractal surface. *Physics of Fluids*, 2016, 28(8): 082001.
- Plimpton, S. Fast parallel algorithms for short-range molecular dynamics. *Journal of Computational Physics*, 1995, 117(1): 1-19.
- Qian, J., Wu, H., Wang, F. Molecular geometry effect on gas transport through nanochannels: Beyond Knudsen theory. *Applied Surface Science*, 2023, 611: 155613.
- Qi, Z., Wang, Y., He, H., et al. Wettability alteration of the quartz surface in the presence of metal cations. *Energy & Fuels*, 2013, 27(12): 7354-7359.
- Ren, S., Shen, F., Yang, S., et al. Analysis and calculation of threshold pressure gradient based on capillary bundle. *Mathematical Problems in Engineering*, 2021, 2021(1): 5559131.
- Rodrigues, H. T., Pereyra, E., Sarica, C. Pressure effects on low-liquid-loading oil/gas flow in slightly upward inclined pipes: Flow pattern, pressure gradient, and liquid holdup. *SPE Journal*, 2019, 24(5): 2221-2238.
- Shahbabaie, M., Kim, D. Advances in nanofluidics for water purification and filtration: Molecular dynamics (MD) perspective. *Environmental Science: Nano*, 2021, 8(8): 2120-2151.
- Siu, S. W., Pluhackova, K., Böckmann, R. A. Optimization of the OPLS-AA force field for long hydrocarbons. *Journal of Chemical Theory and Computation*, 2012, 8(4): 1459-1470.
- Su, H. A flow model reflecting dynamic kick-off pressure gradient for low permeability reservoirs. *Journal of Southwest Petroleum University (Science & Technology Edition)*, 2015, 37(6): 105-111. (in Chinese)
- Sun, S., Liang, S., Liu, Y., et al. A review on shale oil and gas characteristics and molecular dynamics simulation for the fluid behavior in shale pore. *Journal of Molecular Liquids*, 2023, 376: 121507.
- Sutera, S. P., Skalak, R. The history of Poiseuille's law. *Annual Review of Fluid Mechanics*, 1993, 25: 1-20.
- Tomy, A. M., Dadzie, S. K. Diffusion-slip boundary conditions for isothermal flows in micro-and nano-channels. *Micromachines*, 2022, 13(9): 1425.
- Wang, F., Zhao, Y. Slip boundary conditions based on molecular kinetic theory: The critical shear stress and the energy dissipation at the liquid-solid interface. *Soft Matter*, 2011, 7(18): 8628-8634.
- Wang, H., Wang, J., Wang, X., et al. Multi-scale insights on the threshold pressure gradient in low-permeability porous media. *Symmetry*, 2020, 12(3): 364.
- Wang, L., Tang, H., Lv, D., et al. An experimental study of threshold pressure gradient in low permeability reservoir. *Petroleum Geology and Recovery Efficiency*, 2011, 18: 97-100. (in Chinese)
- Wang, S., Liang, Y., Feng, Q., et al. Sticky layers affect oil transport through the nanopores of realistic shale kerogen. *Fuel*, 2022, 310: 122480.
- Wang, W., Xu, J., Zhan, S., et al. Multi-component oil-water two phase flow in quartz and kerogen nanopores: A molecular dynamics study. *Fuel*, 2024, 362: 130869.
- Wu, T., Pan, Z., Liu, B., et al. Laboratory characterization of shale oil storage behavior: A comprehensive review. *Energy & Fuels*, 2021, 35(9): 7305-7318.
- Xu, H., Yu, H., Fan, J., et al. Enhanced gas recovery in kerogen pyrolytic pore network: Molecular simulations and theoretical analysis. *Energy & Fuels*, 2021, 35(3): 2253-2267.
- Yu, H., Xu, H., Fan, J., et al. Transport of shale gas in microporous/nanoporous media: Molecular to pore-scale simulations. *Energy & Fuels*. 2020a, 35(2): 911-943.
- Yu, H., Xu, H., Xia, J., et al. Nanoconfined transport characteristic of methane in organic shale nanopores: The applicability of the continuous model. *Energy & Fuels*, 2020b, 34(8): 9552-9562.
- Zhang, M., Zhao, P., Li, P., et al. Designing biomimic two-dimensional ionic transport channels for efficient ion sieving. *ACS Nano*, 2021, 15(3): 5209-5220.
- Zhang, S., Shen, L., Deng, H., et al. Ultrathin membranes for separations: A new era driven by advanced nanotechnology. *Advanced Materials*, 2022, 34(21): 2108457.
- Zhang, Y. The flow factor approach model for the fluid flow in a nano channel. *International Journal of Heat and Mass Transfer*, 2015, 89: 733-742.
- Zhu, C., Guo, W., Li, Y., et al. Effect of occurrence states of fluid and pore structures on shale oil movability. *Fuel*, 2021, 288: 119847.